

JGR Space Physics

RESEARCH ARTICLE

10.1029/2020JA028883

Key Points:

- Occasionally more than one auroral substorm develops simultaneously at different magnetic local times leading to the formation of double auroral bulges
- It is suggested that the initiation of auroral substorms is a local process, and there is no global reference frame for their development
- Even with double auroral bulges, the overall magnetosphere-ionosphere current system is represented by one globally coherent system

Supporting Information:

Supporting Information may be found in the online version of this article.

Correspondence to:

S. Ohtani,
ohtani@jhupl.edu

Citation:

Ohtani, S., Gjerloev, J. W., McWilliams, K. A., Ruohoniemi, J. M., & Frey, H. U. (2021). Simultaneous development of multiple auroral substorms: Double auroral bulge formation. *Journal of Geophysical Research: Space Physics*, 126, e2020JA028883. <https://doi.org/10.1029/2020JA028883>





Received 29 OCT 2020

Accepted 30 APR 2021

© 2021. The Authors.

This is an open access article under the terms of the [Creative Commons Attribution License](https://creativecommons.org/licenses/by/4.0/), which permits use, distribution and reproduction in any medium, provided the original work is properly cited.

Simultaneous Development of Multiple Auroral Substorms: Double Auroral Bulge Formation

S. Ohtani¹ , J. W. Gjerloev^{1,2} , K. A. McWilliams³ , J. M. Ruohoniemi⁴ , and H. U. Frey⁵ 

¹The Johns Hopkins University Applied Physics Laboratory, Laurel, MD, USA, ²Faculty for Physics and Technology, University of Bergen, Bergen, Norway, ³Institute of Space and Atmospheric Studies, University of Saskatchewan, Saskatoon, Saskatchewan, Canada, ⁴Bradley Department of Electrical and Computer Engineering, Virginia Polytechnic Institute and State University, Blacksburg, VA, USA, ⁵Space Sciences Laboratory, University of California, Berkeley, CA, USA

Abstract The expansion phase of auroral substorms is characterized by the formation of an auroral bulge, and it is generally considered that a single bulge forms following each substorm onset. However, we find that occasionally two auroral intensifications take place close in time but apart in space leading to the formation of double auroral bulges, which later merge into one large bulge. We report three such events. In those events the westward auroral electrojet intensified in each auroral bulge, and geosynchronous magnetic field dipolarized in the same sector. It appears that two substorms took place simultaneously, and each substorm was accompanied by the formation of its own substorm current wedge system. This finding strongly suggests that the initiation of auroral substorms is a local process, and there is no global reference frame for their development. For example, ideas such as (i) the auroral breakup takes place in the vicinity of the Harang reversal and (ii) the westward traveling surge maps to the interface between the plasma sheet and low-latitude boundary layer, do not necessarily hold for every substorm. Even if those ideas may be suggestive of causal magnetospheric processes, the reference structures themselves are probably not essential. It is also found that despite the formation of two distinct auroral bulges, the overall magnetosphere-ionosphere current system is represented by one globally coherent system, and we suggest that its structure is determined by the relative intensities and locations of the two substorm current wedges that correspond to the individual auroral bulges.

1. Introduction

Auroral substorms show a recurrent sequence of auroral development on the nightside (Akasofu, 1964). The initial brightening very often takes place at premidnight (Frey et al., 2004; Liou et al., 2001), then auroral intensification expands poleward as well as westward and eastward forming an auroral bulge, which characterizes the substorm expansion phase. Although auroral bulges may form at different locations in different sizes, various features such as auroral electrojets, field-aligned currents (FACs), convection flows, and particle precipitation are distributed relative to auroral bulges (e.g., Fujii et al., 1994; Gjerloev & Hoffman, 2001, 2014). In other words, for classical (i.e., Akasofu-type) auroral substorms, auroral bulges serve as a reference frame of substorm-related magnetosphere-ionosphere (M-I) coupling.

One perception that is widely shared, but seldom addressed explicitly, is that a single auroral bulge forms following each substorm onset. Substorm onsets are often followed by another onset, and occasionally, more than one auroral bulge exists at a given time. Therefore, the coexistence of multiple bulges does not necessarily mean that they form simultaneously. On the other hand, if substorms are triggered by a local magnetospheric process, it should be possible that more than one substorm takes place concurrently at different locations, and accordingly, multiple auroral bulges form simultaneously even if such observations have not been documented in the past (to our best knowledge). Otherwise, the occurrence of substorms must be somehow constrained globally so that only one substorm can take place at a given moment.

In the present study, we report three events in which we found two auroral bulges developed simultaneously. We characterize those events in the context of M-I coupling and discuss their implications for substorm dynamics. In Section 2 we briefly examine each event. In Section 3 we discuss the results and address new insights the present study provides into substorm initiation and development. We summarize the overall study in Section 4.

2. Observations

For selecting multiple-auroral bulge formation events, we used global auroral image data taken by the wideband imaging camera (WIC) of the far ultraviolet imager (FUV) onboard the IMAGE satellite (Mende et al., 2000). The IMAGE satellite was launched in March 2000 into an elliptical polar orbit of $1,000 \text{ km} \times 7.2 R_E$ with an orbital period of $\sim 14 \text{ h}$. The FUV instrument measured aurora in every two minutes. We used the WIC images that were provided to SuperMAG and implemented in its polar plot function so that the auroral images can be browsed along with the polar distribution of equivalent currents. Strictly speaking, what is shown in the SuperMAG polar diagrams are ground magnetic disturbance vectors rotated clockwise by 90° , but if converted to the current intensity, they may be considered as a proxy of equivalent currents (Nagata & Fukushima, 1971). For a ground magnetic disturbance of 100 nT, the corresponding current intensity is 160 mA/m (160 A/km) provided that it can be attributed to an infinitely extending ionospheric current, or 110 mA/m (110 A/km) if one third of the ground magnetic disturbance is caused by a current induced under the ground. In the rest of this study we refer to such rotated magnetic vectors as equivalent currents; this should not affect this study in any sense since we examine those vectors only qualitatively for addressing the development of the westward auroral electrojet and the formation of a wedge current system.

The auroral oval is usually structured in longitude to some extent, and we found many events in which the initial auroral intensification started at multiple, but longitudinally clustered, locations, and they immediately merged into one auroral bulge. For such events we cannot tell whether the initial auroral enhancement represents a single onset with internal structures or multiple onsets that took place concurrently in the same area. However, occasionally another auroral bulge started to form at a different local time (i.e., apart from the first bulge by more than its longitudinal extent) while the first bulge was still growing in size. In the following we examine three such events, which we found by visually searching the IMAGE FUV/WIC data during the interval of September 2000 to March 2001. Whereas multiple bulge formation is obvious in the first two events, the last event is more complex but provides additional insight.

2.1. Event on September 15, 2000

The first event that we examine took place on September 15, 2000. Figure 1a shows the three components of the interplanetary magnetic field (IMF) in the geocentric solar magnetospheric (GSM) coordinate system propagated to Earth (by shifting the OMNI data by additional 5 min), whereas Figure 1b shows SMU00 and SML00 (solid lines) along with the original SMU and SML indices (dotted lines). SMU and SML are SuperMAG equivalents to the AU and AL indices, respectively (Gjerloev, 2012; Newell & Gjerloev, 2011). SMU00 and SML00 are the same as SMU and SML but derived from stations located in the midnight quadrant, that is, within 6 hours in magnetic local time (MLT) centered at $\text{MLT} = 00$ (Ohtani et al., 2021). SML00 is more suitable for examining substorm activity on the nightside. Figure 2 shows the polar maps of equivalent currents (green vectors) along with IMAGE FUV/WIC auroral images every two minutes during 2058–2108 UT, the interval marked by the horizontal segment in Figure 1b; see Movie S1 for an extended interval, 2050–2120 UT. Each panel shows the last available auroral image taken at the time indicated in the parentheses.

We can find a bright spot at $\text{MLT} = \sim 01$ in the panel of 2100 UT (Figure 2b) but not in the panel of 2058 UT (Figure 2a). SML00 started to decrease gradually at 2100 UT (Figure 1b). Later we will find that a substorm-related magnetic disturbance started at 2059 UT in the subauroral zone, and therefore we identify 2059 UT as a substorm onset. The onset was preceded by a period of southward IMF B_z with its minimum below -10 nT , and it took place as all three IMF components were gradually changing (Figure 1a).

The postmidnight auroral spot expanded in the next two minutes; see the panel of 2102 UT (Figure 2c). In the same panel we can find a hint of another auroral intensification starting at $\text{MLT} = 21\text{--}23$, which became far more noticeable by 2104 UT (Figure 2d). This new auroral intensification took place within a few minutes after the start of the postmidnight intensification. Each of the premidnight and postmidnight active regions expanded forming distinct auroral bulges (Figures 2e and 2f). At the same time the westward auroral electrojet intensified in each bulge as shown by the enhancements of equivalent currents, and SML00 fell below -600 nT at 2109 UT in 10 min after the onset (Figure 1b). Although this SML00 reduction alone may look like a single substorm, the auroral images clearly show that two distinct substorms took

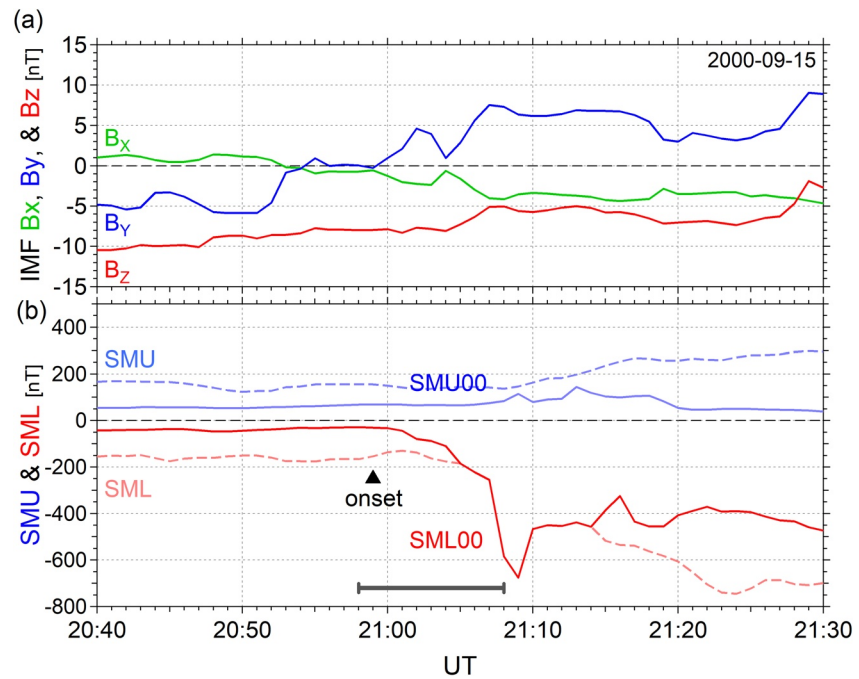


Figure 1. (a) IMF B_x (green), B_y (blue), and B_z (red) components in the GSM coordinate system propagated to Earth (with an additional 5-min time shift from the OMNI data set) during the interval 0520–0610 UT on September 15, 2000. (b) SMU00 (blue solid) and SML00 (red solid) indices along with the original SMU (blue dotted) and SML (red dotted) indices. The horizontal bar indicates the interval examined in Figure 2.

place concurrently. By 2112 UT the two bulges merged into one large bulge, which extended over the entire nightside (see Movie S1).

Now we examine midlatitude ground magnetic signatures to address the MLT distribution and development of the substorm current system. Figure 3 shows three magnetic components observed at three sub-auroral zone ground stations, Valentia (VAL; 49.8°N in magnetic latitude (MLat)), Brorfelde (BFE; MLat = 52.1°N), and Borok (BOR; MLat = 53.9°N) located from the west to the east in the European sector. The locations of these stations are marked in Figure 2a. N, E, and Z are directed northward, eastward, and vertically downward, respectively, and N and E can be regarded as the disturbance parts of the conventional H and D (in nT) magnetic components (Gjerloev, 2012).

At BOR, the station located most eastward and closest to the initial postmidnight auroral brightening, N and E started to decrease and increase, respectively, at 2059 UT; this is the reason we identify 2059 UT as substorm onset. The substorm current wedge (SCW) model suggests that BOR was located to the west of the upward FAC of the SCW (Clauer & McPherron, 1974), which is consistent with the location of BOR relative to the postmidnight auroral intensification.

At the other two stations, in contrast, E was initially flat probably because those stations were located farther outside of the SCW. However, E started to increase at 2107 UT at VAL and at 2108 UT at BFE, whereas at BOR, E started to decrease. At the same time N started to increase at BFE and BOR, but it did not change clearly at VAL. These observations suggest that in association with the premidnight auroral intensification, a new SCW formed with its center between BFE and BOR in longitude and its western edge around the VAL meridian. This inference is consistent with the fact that the westward auroral electrojet was most intense before midnight (MLT = ~2330) at 2108 UT (Figure 2f). One reservation for this interpretation is that we cannot tell, from the ground magnetic disturbances, how FACs were distributed in the midnight sector, where the downward FAC of this premidnight SCW and the upward FAC of the postmidnight SCW might have partially overlapped. We will discuss in Section 3 the global distribution of the M-I current system associated with multiple bulge formation.

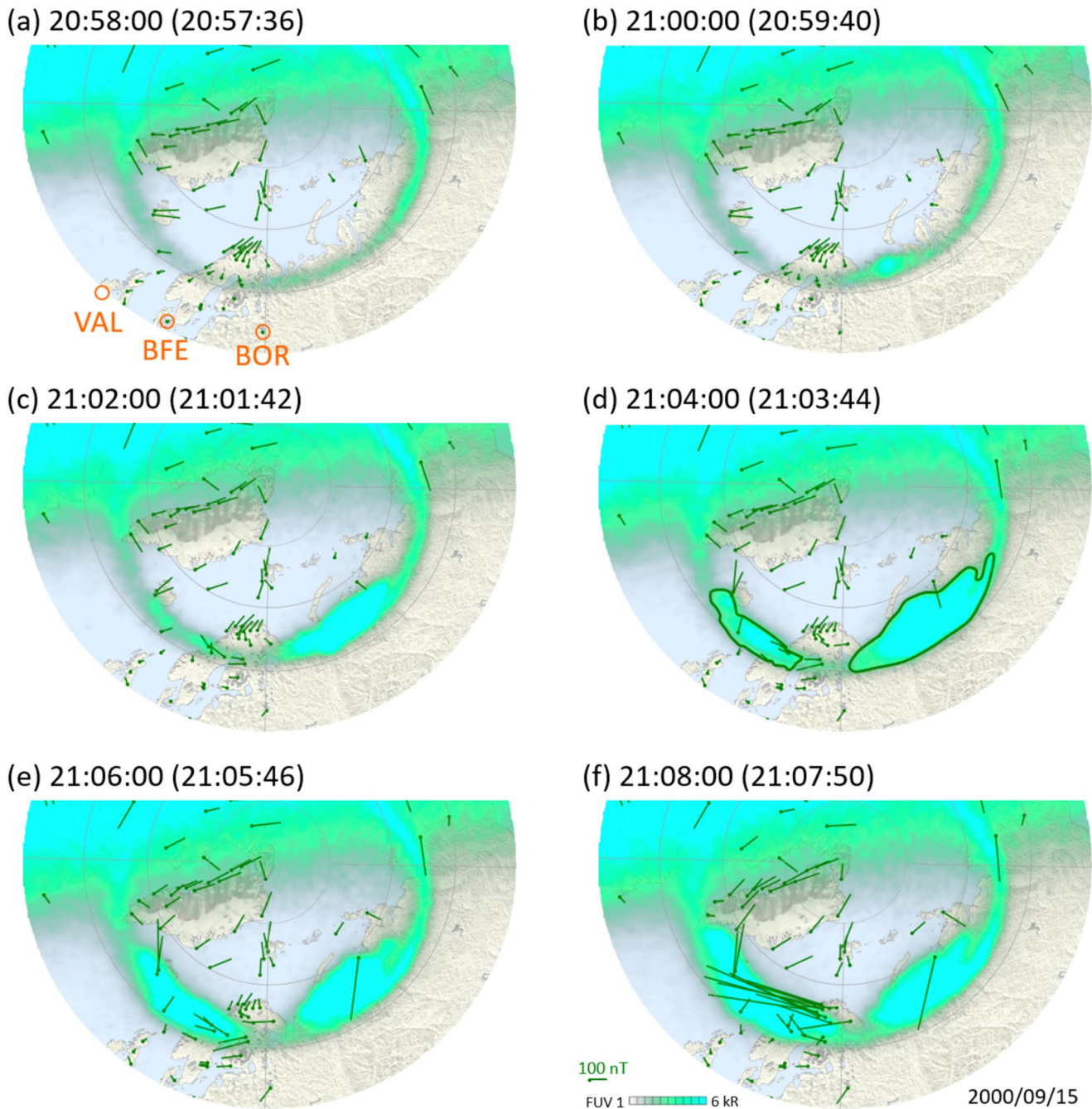


Figure 2. Polar maps of equivalent currents (ground magnetic disturbance vectors rotated clockwise by 90°) every two minutes from 2058 to 2108 UT on September 15, 2000 along with IMAGE FUV/WIC auroral images taken at the times in the parentheses. All panels share the reference vector shown in Figure 2f, the length of which, 100 nT, corresponds to a current intensity of 160 mA/m or 160 A/km if it can be attributed to an infinitely extending ionospheric current. The locations of Valentia (VAL), Brorfelde (BFE), and Borok (BOR) ground stations are marked in Figure 2a. Sun is to the top. The two green contours in Figure 2d correspond to the magenta contours in Figure 4.

Now we examine ionospheric convection in this event. Figures 4a and 4b show the polar maps of ionospheric convection derived from measurements made by SuperDARN radars (Greenwald et al., 1985) during the 2-min intervals of 2058–2100 and 2102–2104 UT, right before and after the start of the premidnight auroral enhancement. The contours indicate lines of constant electrostatic potential at every 6 kV, which were obtained by fitting spherical harmonics to measurements with constraints from a statistical model (Ruohoniemi & Baker, 1998). Convection velocities are shown wherever line-of-sight velocity measurements are

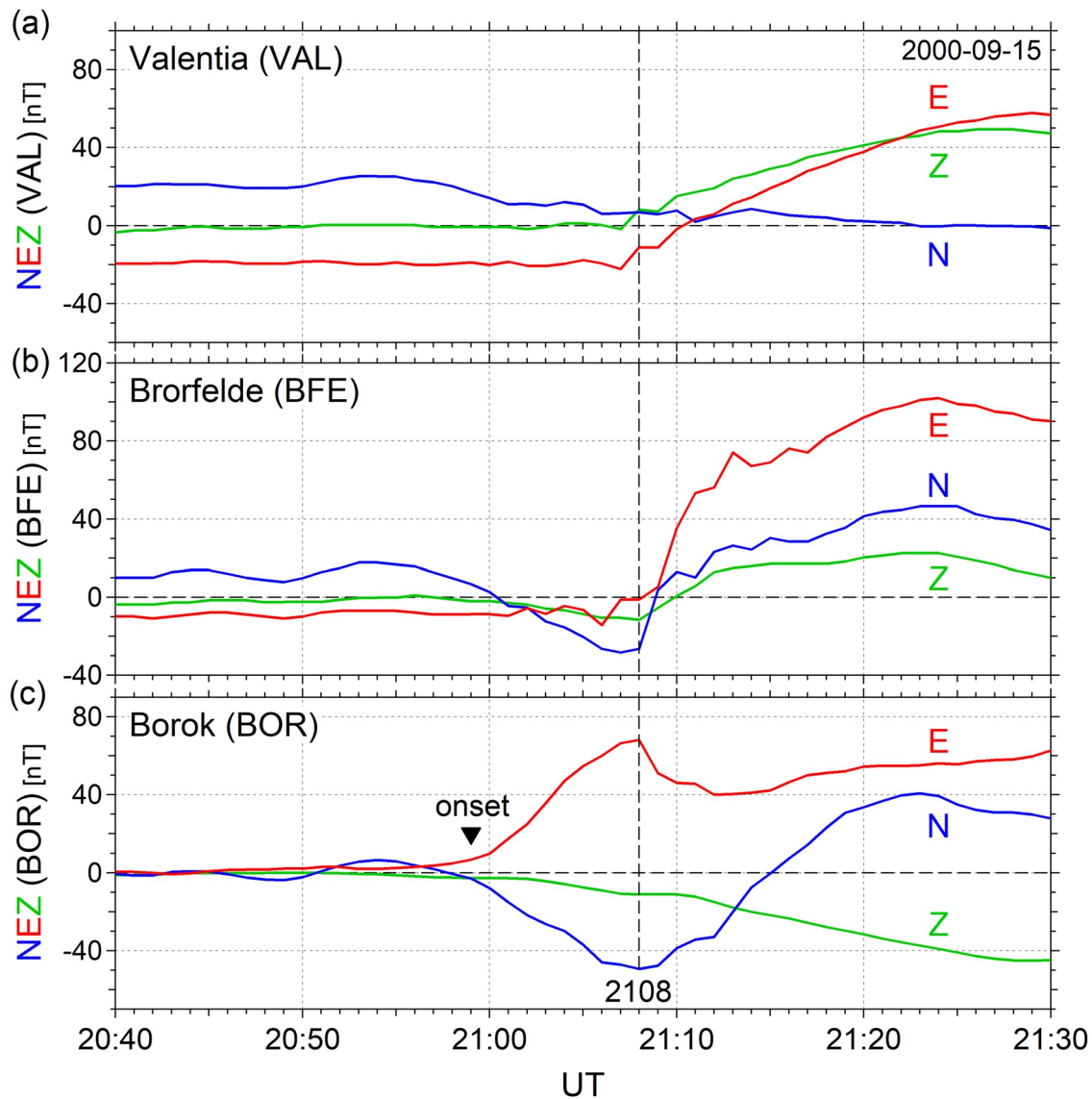


Figure 3. N (blue), E (red), and Z (green) magnetic disturbances observed at: (a) Valentia (VAL), (b) Brorfelde (BFE), and (c) Borok (BOR) during the interval 2040–2130 UT on September 15, 2000.

available from at least one radar; each velocity is reconstructed from the measured line-of-sight velocity and its perpendicular component obtained from the spherical harmonic fit. The two magenta contours on the nightside show the green-contoured areas of auroral intensification in Figure 2d; we disregarded any deformation due to the magnetic mapping from the E region (for IMAGE FUV/WIC) to the F region (for SuperDARN).

The overall convection pattern consisted of two cells of comparable sizes as expected from the observed IMF orientation with IMF B_y smaller than southward IMF B_z in magnitude (Figure 1a). For each 2-min interval, the demarcation between the dawn and dusk convection cells was located at premidnight, which indicates that the postmidnight auroral intensification was located in the dawn cell.

In summary, in the September 15, 2000 event, two auroral bulges started to form within a few minutes following substorm onset. The first bulge formed at postmidnight in the dawn convection cell, then the second bulge formed at premidnight in the dusk convection cell. Each bulge was accompanied by the formation of its own SCW system. Apparently two distinct substorms took place concurrently in this event.

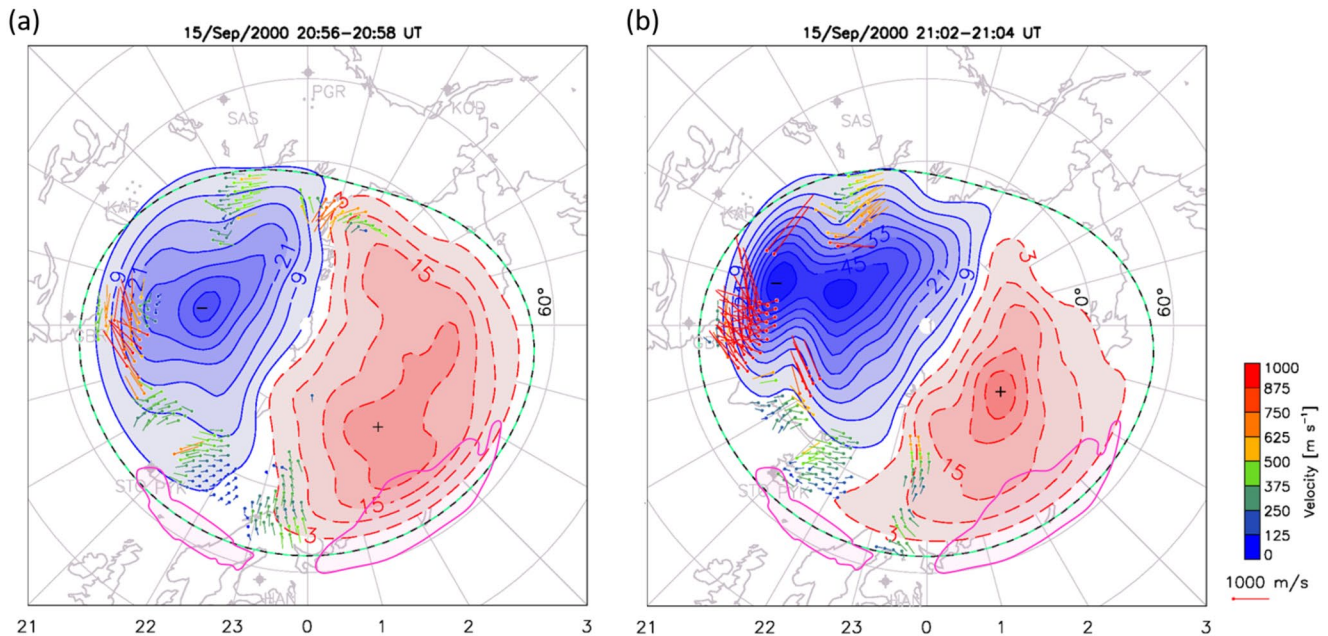


Figure 4. Polar maps of ionospheric convection derived from measurements made by SuperDARN radars during the intervals: (a) 2058–2100 and (b) 2102–2104 UT on September 15, 2000. The contours indicate lines of constant electrostatic potential at every 6 kV, and the vectors indicate convection velocities, derived from the fitting where line-of-sight velocity measurements are available. The two magenta contours on the nightside correspond to the green contours in Figure 2d showing the areas of auroral intensification.

2.2. Event on September 30, 2000

The second event that we examine took place on September 30, 2000. Figure 5 shows the IMF data (top) and SMU00 and SML00 along with SMU and SML (bottom) for this event. Figure 6 shows the polar maps of equivalent currents and IMAGE FUV/WIC auroral images in the same format as Figure 2. IMF B_z was strongly negative (~ -10 nT) before the event (Figure 5a), and accordingly, the magnitudes of both SMU and SML were around 300 nT (Figure 5b) reflecting intense auroral electrojets in the flank sectors (Figure 6a). In the midnight sector, however, the auroral electrojets were much weaker, and therefore, SMU00 and SML00 serve as better measurements of nightside substorm activity.

A bright auroral area at MLT = ~ 22 can be recognized in the panel of 0535 UT (Figure 6b) but not in the panel of 0533 UT (Figure 6a). However, this earlier image also reveals a corresponding, but significantly weaker and spatially confined, intensification if we use a color code with a lower saturation level (not shown). At Pinawa (PIN; MLat = 60.7° N; marked in Figure 6a), which was located near the eastern edge of the bright spot, both N and Z started to decrease at 0532 UT (Figure 7b), and at the same time a positive bay started at Boulder (BOU; MLat = 49.1° N; marked in Figure 6a) in the same sector (Figure 7c). Therefore, although SML00 started to decrease at 0539 UT (Figure 5b), we identify the onset of this substorm event at 0532 UT.

While this premidnight auroral intensification expanded forming a small bulge in the next several minutes, another bulge emerged at postmidnight by 0541 UT (Figure 6d). The area of this new auroral intensification exceeded that of the premidnight bulge within two minutes (Figure 6e), and the westward electrojet enhanced simultaneously as indicated by the decrease in N at Poste de la Baleine (PBQ; MLat = 65.8° N; marked in Figure 6a) located around the poleward edge of the postmidnight auroral bulge (Figure 7a). Then the two bulges merged into one large bulge extending over the entire midnight sector (Figure 6f) and continued to expand (see Movie S2). As this merged bulge developed further, SML00 reached -800 nT at 0550 UT (Figure 5b). Whereas in the September 15, 2000 event the auroral bulge formed first at postmidnight and then at premidnight (Section 2.1), in the present event the two bulges formed in the reverse order.

We now examine nightside geosynchronous magnetic signatures observed in this event. Figures 8a and 8b show the VDH magnetic components measured by the GOES 10 (G10) and GOES 8 (G08) satellites,

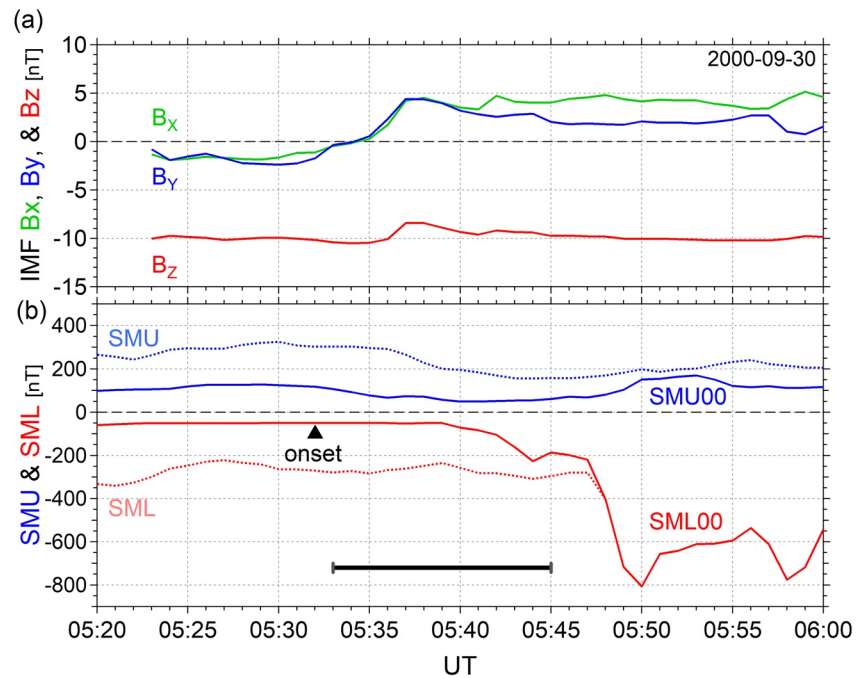


Figure 5. (a) IMF B_x (green), B_y (blue), and B_z (red) components in the GSM coordinate system propagated to Earth (with an additional 5-min time shift from the OMNI data set) during the interval 0520–0600 UT on September 30, 2000. (b) SMU00 (blue solid) and SML00 (red solid) indices along with the original SMU (blue dotted) and SML (red dotted) indices. The horizontal bar indicates the interval examined in Figure 6.

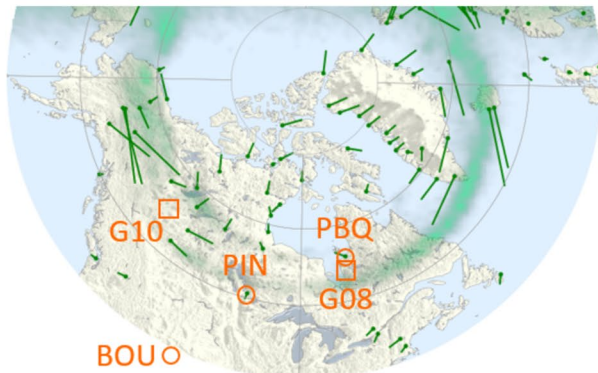
respectively; V is radially outward, D is azimuthally eastward, and H is parallel to the dipole axis positive northward. G10 was located at geographic longitude of 135.3°W ($LT = UT - 9.0$) and $MLat = 4.8^\circ$, and G08 was located at geographic longitude of 74.8°W ($LT = UT - 5.0$) and $MLat = 10.2^\circ$. The footprints of G08 and G10 at 100 km in altitude are marked in Figure 6a, which were located near the premidnight and post-midnight auroral bulges, respectively. For calculating their locations, we used the T89 model (Tsyganenko, 1989) for $K_p = 3$, for which V and H are -28.2 and 64.0 nT at G10, and -74.5 and 49.5 nT at G08, but the measured magnetic field was more stretched especially before dipolarizations (Figure 8), and therefore, the actual footprints should be located more equatorward; nevertheless, those calculated footprint locations should be sufficient for addressing observed signatures in the context of the bulge development.

At G10, H (red) started to increase at 0532 UT coincidentally with the formation of the premidnight auroral bulge (Figure 8a). The subsequent H increase was gradual but persistent for more than 20 min. At the same time D (green) changed positively, which can be attributed to an upward FAC on the poleward side of the satellite. This is consistent with the G10 footprint near the premidnight bulge. It is therefore suggested that a SCW formed in association with the premidnight auroral bulge.

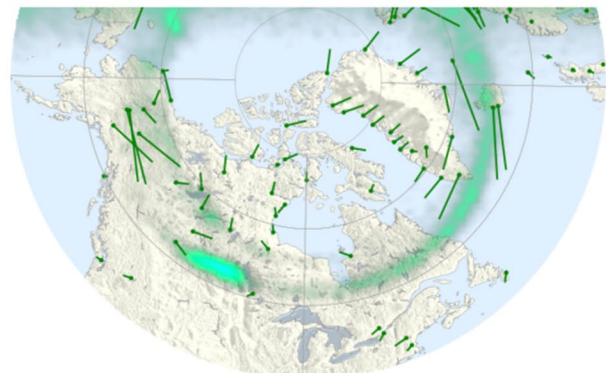
At G08 H and $|V$ (blue) started to increase and decrease, respectively, at 0539 UT (Figure 8b). That is, the local magnetic field changed from a stressed to a more dipolar configuration. This dipolarization onset coincided with the initial formation of the postmidnight auroral bulge, which took place between 0538:22 (Figure 6c) and 0540:24 UT (Figure 6d). The G08 dipolarization was sharper than the one at G10 possibly reflecting the more rapid expansion of the postmidnight auroral bulge. The G08 D component made a transient negative excursion for the first few minutes, presumably responding to a newly forming upward FAC (located poleward of G08) associated with the postmidnight auroral bulge, but immediately returned to the pre-onset levels and fluctuated largely.

Figure 9 shows the polar maps of ionospheric convection during the 2-min intervals of 0536–0538 and 0542–0544 UT, right before and after the formation of the postmidnight bulge formation. In this event, the Harang reversal was noticeable as shown by the potential contours extending from $MLT = 21$ to midnight, around which the measured convection flows rotated clockwise. The nightside magenta contours show the

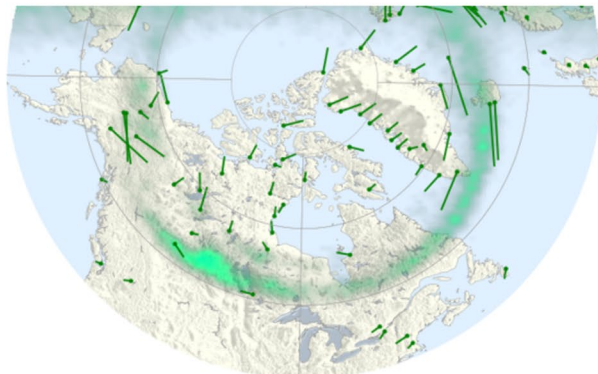
(a) 05:33:00 (05:32:16)



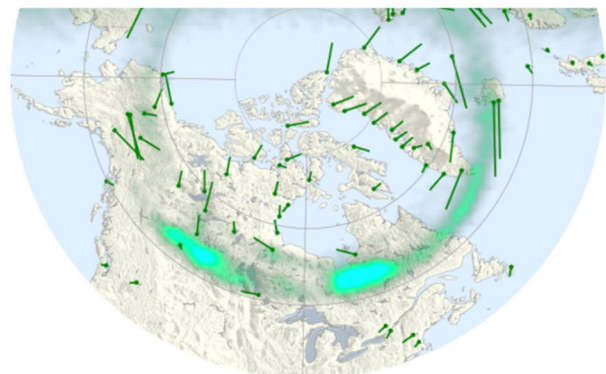
(b) 05:35:00 (05:34:16)



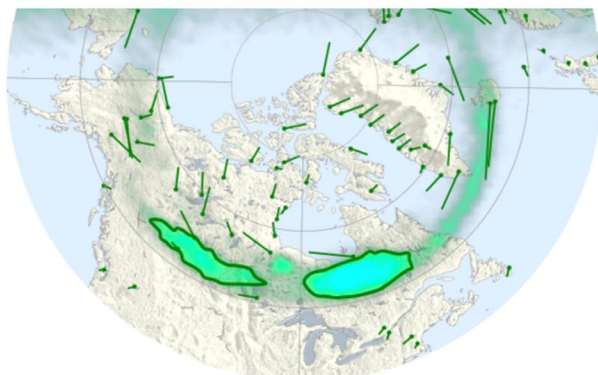
(c) 05:39:00 (05:38:22)



(d) 05:41:00 (05:40:24)



(e) 05:43:00 (05:42:28)



(f) 05:45:00 (05:44:30)

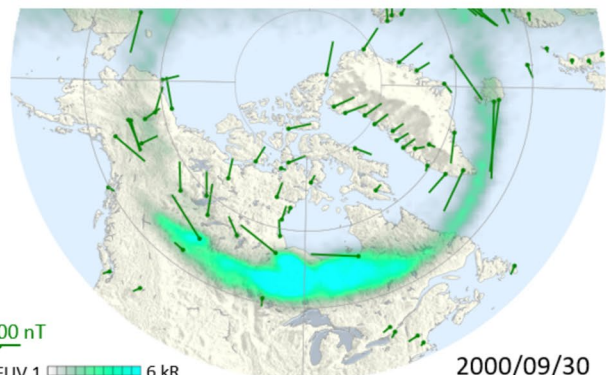


Figure 6. Polar maps of equivalent currents (ground magnetic disturbance vectors rotated clockwise by 90°) from 0533 to 0545 UT on September 30, 2000 along with IMAGE FUV/WIC auroral images taken at the times in the parentheses. Sun is to the top. The footprints of G08 and G10 as well as Poste de la Baleine (PBQ), Pinawa (PIN), and Boulder (BOU) ground stations are marked in Figure 6a (see text). The two green contours in Figure 6c correspond to the magenta contours in Figure 9.

areas of auroral intensification at 0542:28 UT (Figure 6e), which indicate that whereas the premidnight auroral bulge was located in the dusk convection cell, the postmidnight auroral bulge formed around the demarcation between the dusk and dawn convection cells.

In summary, in the September 30, 2000 event, two auroral bulges developed subsequently (in 5 min) at the early stage of the substorm expansion phase. The formation of each bulge was accompanied by a geosynchronous dipolarization in the corresponding sector. The premidnight bulge formed in the dusk convection

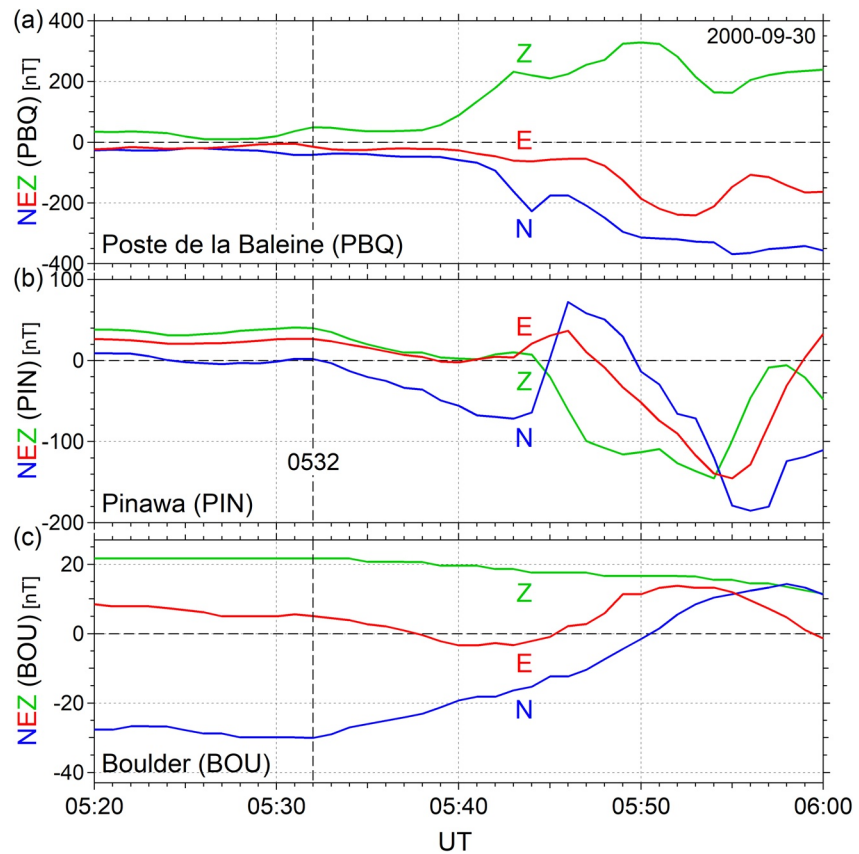


Figure 7. N (blue), E (red), and Z (green) magnetic disturbances observed at: (a) Poste de la Baleine (PBQ), (b) Pinawa (PIN), and (c) Boulder (BOU) during the interval 0520–0600 UT on September 30, 2000.

cell as we found for the September 15, 2000 event (Section 2.1), and the postmidnight bulge formed near the demarcation between the dusk and dawn convection cells.

2.3. Event on March 18, 2001

In this subsection we briefly examine the last event, which took place on March 18, 2001. This event is more complex than the previous two events, but it reveals additional features. Figure 10 shows the polar maps of equivalent currents along with IMAGE FUV/WIC auroral images every two minutes during 0517–0527 UT. Before this interval, IMF B_z was around -2 nT for more than 2 h, but SML was merely -50 nT, then it started to decrease at 0518 UT (not shown). Overall auroral activity was also low before the event except that minor intensifications took place sporadically around the flanks (a duskside example may be found in Movie S3).

The first sustained auroral enhancement started just before 0517 UT around $MLT = 04$ as shown in Figure 10a. The bright area developed into an auroral bulge in the next 4 min, and the westward auroral electrojet intensified (Figures 10b and 10c). The timing matches the start of the aforementioned SML reduction. At the same time aurora enhanced also in the premidnight sector. Three auroral spots are noticeable at $MLT = 21$ – 23 in Figure 10c, which may be an internal structure of a single intensification. Whereas this auroral enhancement subsequently extended in longitude, its latitudinal expansion was limited. Interestingly, G10 was located in the same MLT sector (as marked in Figure 10a), but as shown in Figure 11a, it did not observe any clear signature of dipolarization; the local H component was basically unchanged until 0532 UT, then it decreased transiently. On the ground, no positive bay signature was observed at Boulder (not shown), even though Boulder ($LT = UT - 7.0$ as marked in Figure 10a) was in the same sector as the premidnight auroral intensification. It is possible that this premidnight auroral intensification was related to the

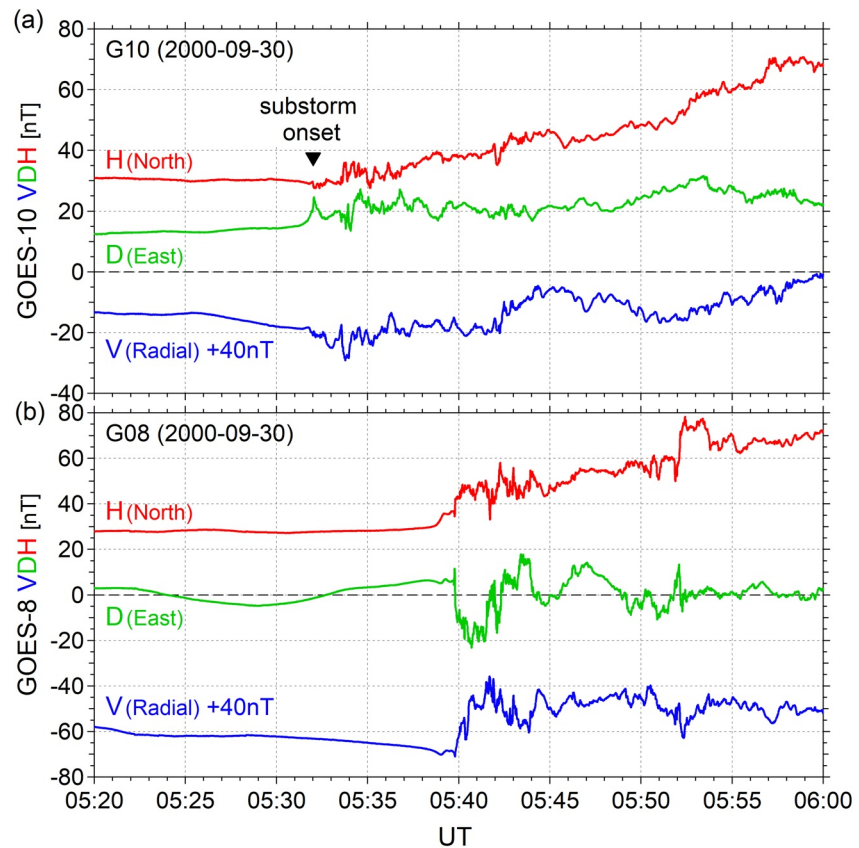


Figure 8. (a) G10 and (b) G08 magnetic field measurements in VDH during the interval 0520–0600 UT on September 30, 2000.

enhancement of local ionospheric convection rather than to a substorm process; we could not test this idea with SuperDARN data because of the lack of appropriate line-of-sight velocity measurements.

The situation was rather different for the large spot that emerged at postmidnight, at MLT = 00–01, by 0522:21 UT (Figure 10d). The bright auroral area expanded in both longitude and latitude, and the westward auroral electrojet intensified inside (Figures 10e and 10f). G08 had its footprint around this auroral spot (marked in Figure 10a) and observed a sharp dipolarization starting at 0521:28 UT (Figure 11b), simultaneously with the formation of this postmidnight auroral spot. G08 also observed a positive D deviation, which suggests the generation of an upward FAC (on the poleward side of G08) in the sector of this auroral enhancement. Apparently this postmidnight auroral spot was accompanied by typical substorm features, and therefore, it can be regarded as an auroral bulge. This newly formed bulge later merged with the dawnside bulge forming a single active area extending several hours in MLT (see Movie S3).

In summary, during the expansion phase of the March 18, 2001 substorm, two auroral bulges formed simultaneously, one at early dawn and another at postmidnight. The local westward auroral electrojet intensified for each bulge, and a sharp dipolarization was observed for the postmidnight bulge. Another auroral intensification took place in the late evening sector, which, however, likely reflected an enhancement of ionospheric convection rather than a substorm.

3. Discussion

In Section 2, we examined three events in which auroral activation took place at multiple locations at the very early stage of the substorm expansion phase. In general, the auroral oval is rarely uniform in longitude, and there are often multiple active spots or areas of aurora. For example, corresponding to the enhancement of the global two-cell convection before substorm onsets, aurora often enhances at the flanks (Shue

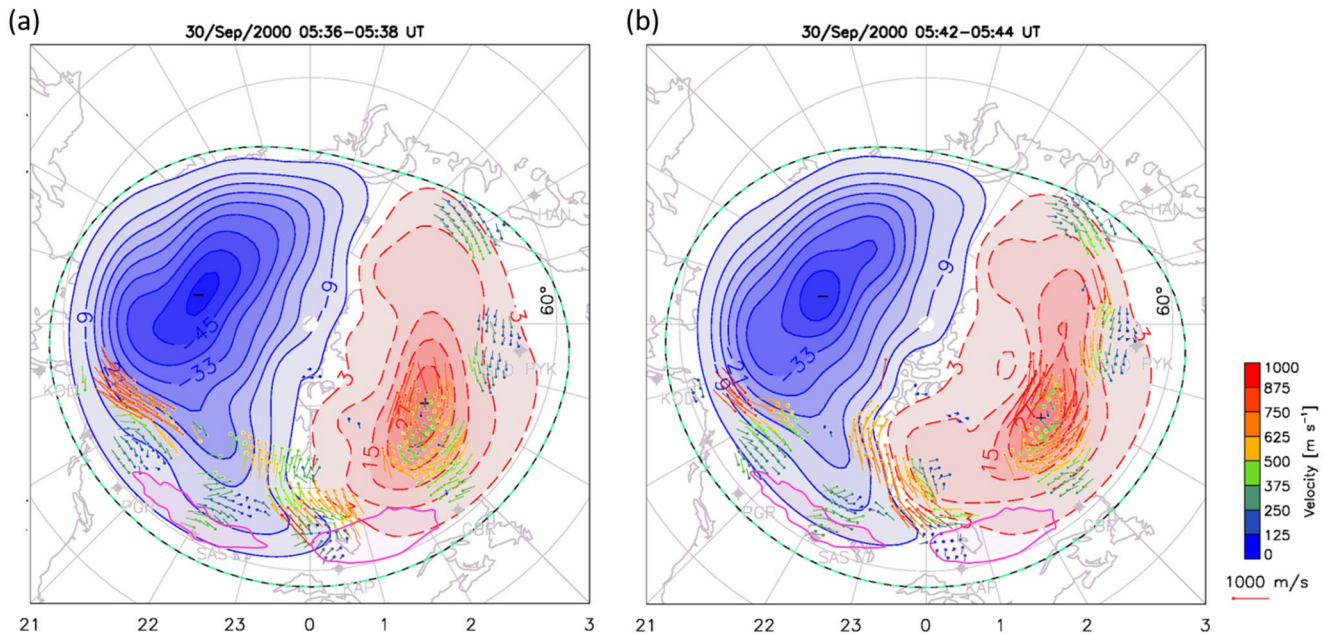


Figure 9. Polar maps of ionospheric convection derived from measurements made by SuperDARN radars during the intervals: (a) 0536–0538 and (b) 0542–0544 UT on September 30, 2000. The contours indicate lines of constant electrostatic potential at every 6 kV, and the vectors indicate convection velocities, derived from the fitting where line-of-sight velocity measurements are available. The two magenta contours on the nightside correspond to the green contours in Figure 6e showing the areas of auroral intensification.

et al., 2002). For multiple-onset substorms, new auroral enhancements may be followed by the formation of a new bulge while a preceding substorm is recovering. We, however, emphasize that the multi-point auroral activation that we reported in Section 2 is distinct from those phenomena in the sense that individual auroral enhancements simultaneously developed into auroral bulges. Since the formation of an auroral bulge is a characteristic feature of auroral substorms, we conclude that substorms can take place simultaneously at more than one location in the M-I system; in each of the three events that we examined, the initial auroral enhancements (i.e., substorm onsets) started with a 2–6 min difference at two locations, but the bulge formation (i.e., substorm expansion phase) took place simultaneously.

In the September 15, 2000 and September 30, 2000 events, SML00 reached -670 and -800 nT, respectively (Figures 1 and 5), and in the March 18, 2001 event SML00 became -340 nT (not shown). Considering that the minimum AL of classical (i.e., Akasofu-type) isolated substorms is typically -400 nT (Gjerloev et al., 2007), we suggest that prior to the substorm onsets of those events, the magnetotail had been loaded with substantial energy.

We found that in those events, each auroral bulge was accompanied by typical substorm features such as a westward electrojet enhancement, midlatitude positive bay, and geosynchronous dipolarization. If substorms are triggered by the braking of a fast plasma flow in the near-Earth region (see, e.g., a review by Kepko et al., 2015), the present result suggests that two fast flows penetrated into the near-Earth region essentially at the same time, and this takes place preferably when the magnetotail is loaded with energy. In general, the magnetotail can accommodate only a limited number of fast flows at a given moment even during the substorm expansion phase (Ohtani, 2019). The typical potential difference across a flow channel is ~ 20 kV, whereas the cross-polar cap potential difference is typically below 100 kV even during very active times (e.g., Ahn et al., 1992; Bristow et al., 2004), and it should be significantly smaller during the substorm growth phase. Therefore, unless the fast flow channel is unusually narrow, the external driving has to be intense for more than one flow channel to coexist right before substorm onset. Furthermore, prior to more intense substorms, the nightside equatorial magnetic field tends to be more depressed in the near-Earth region (Lopez & von Roseninge, 1993), and accordingly, the flux tube entropy is more elevated before substorm onsets. The associated magnetic configuration is more favorable for a fast plasma flow to penetrate deeper into the near-Earth region, which is widely considered as the interchange motion of a depleted flux

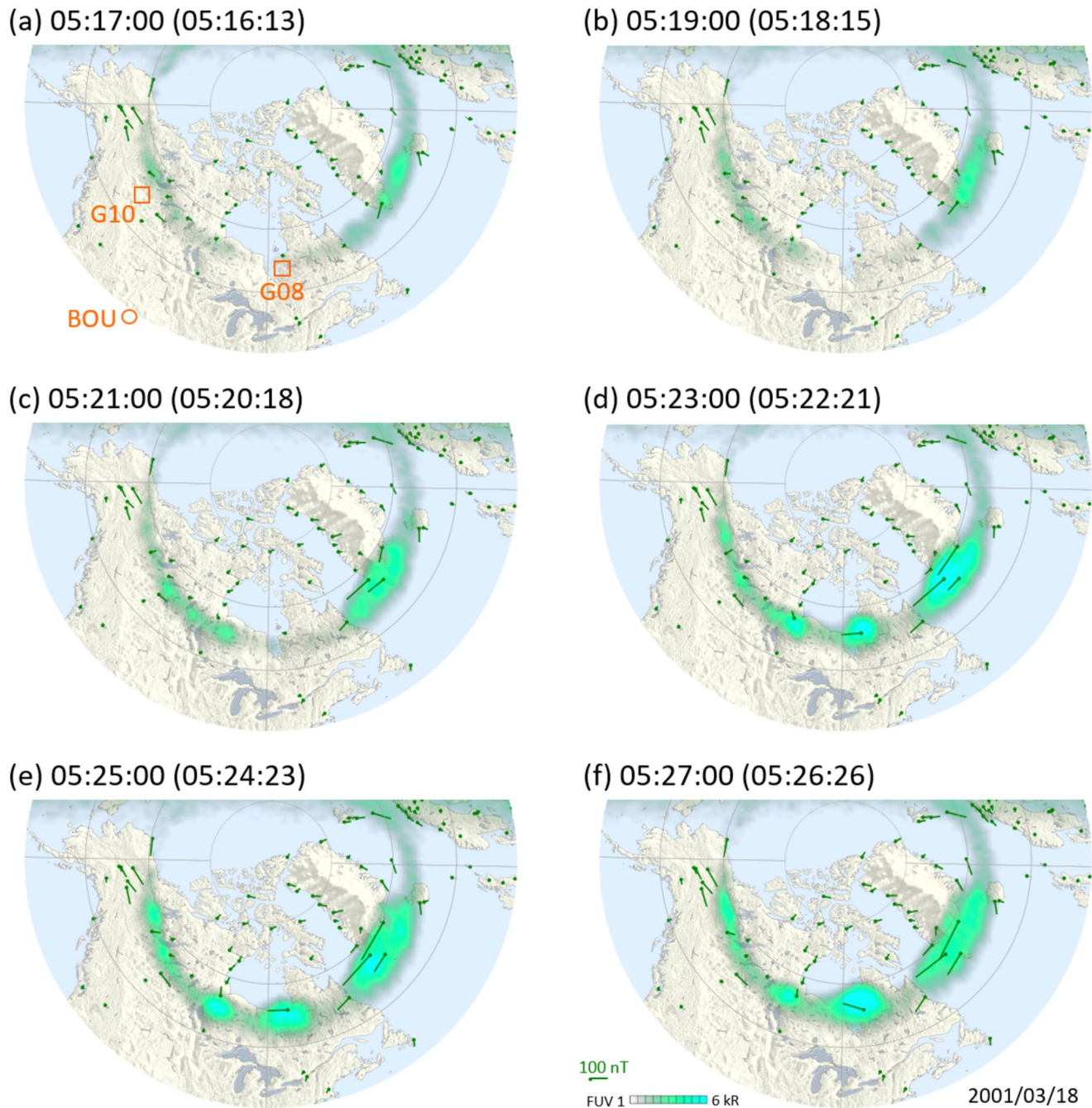


Figure 10. Polar maps of equivalent currents (ground magnetic disturbance vectors rotated clockwise by 90°) every two minutes from 0517 to 0527 UT on March 18, 2001 along with IMAGE FUV/WIC auroral images taken at the times in the parentheses. The footprints of G08 and G10 as well as the location of Boulder (BOU) ground station are marked in Figure 10a. Sun is to the top.

tube (Wolf et al., 2009). Therefore, the double auroral bulge formation may be indicative of the formation of multiple fast flows and subsequent penetration into the near-Earth region.

However, the double bulge formation itself does not preclude the possibility that the substorm is triggered by a local plasma instability (e.g., the ballooning instability). Instead, it suggests that local plasma and magnetic configurations become unstable to a certain instability at more than one location, which is possible if the M-I system was metastable to that instability over a larger area corresponding to more significant energy loading. This remark also applies to the idea of substorm initiation by flow braking since magnetic

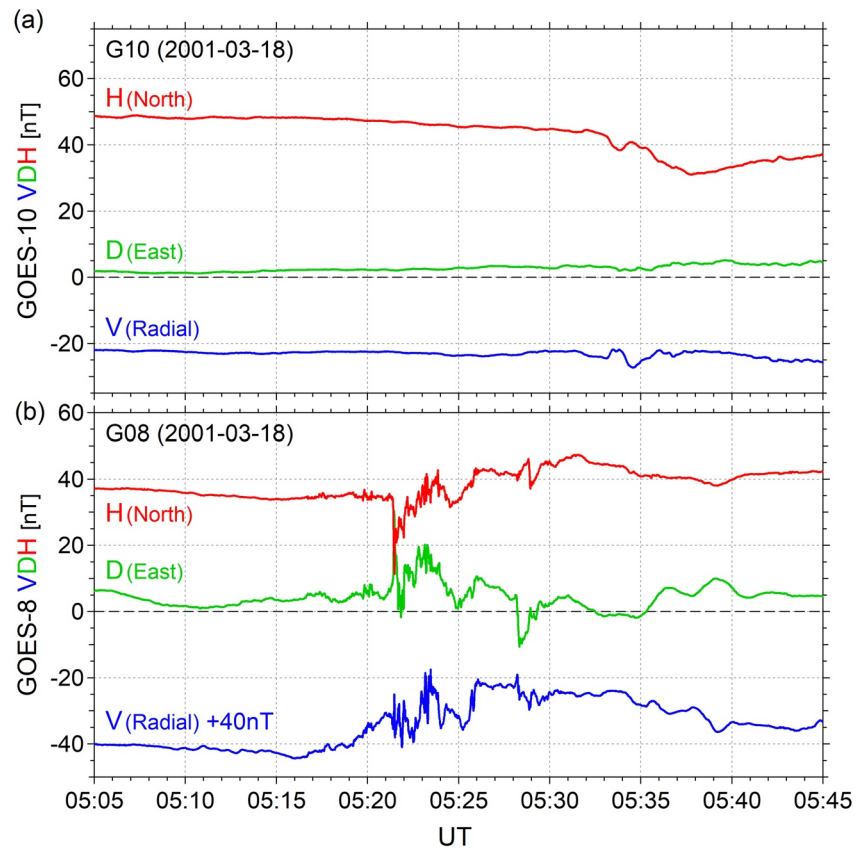


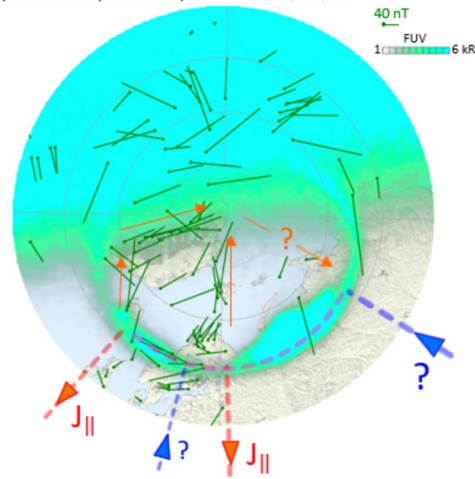
Figure 11. (a) G10 and (b) G08 magnetic field measurements in VDH during the interval 0505–0545 UT on March 18, 2001.

reconnection is widely considered to be the cause of the formation of depleted flux tubes, and for explaining the double auroral bulge formation, the idea requires that magnetic reconnection takes place at multiple locations.

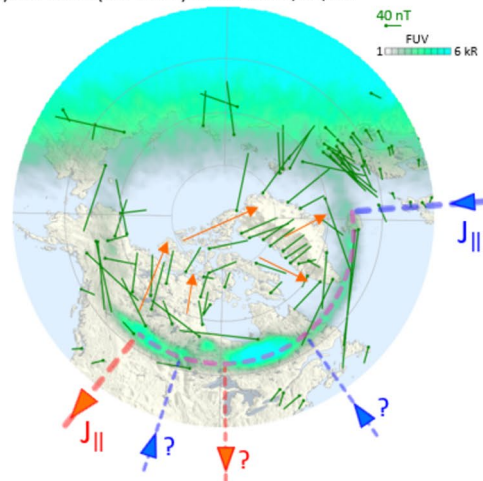
The results of the present study cast new light on the relationship between substorm initiation and global structures of the M-I system, which we discuss here focusing on the Harang reversal and westward traveling surge (WTS). First, our results strongly suggest that there is no necessity for substorm onsets to take place in the vicinity of the Harang reversal. Numerous studies have reported the occurrence of substorm onsets at or near the Harang (convection) reversal (Bristow & Jensen, 2007; Zou et al., 2009). However, Weygand et al. (2008) statistically examined the location of substorm onsets (as defined with IMAGE FUV/WIC images) relative to the Harang reversal (as defined by the vortex center of ionospheric currents) and concluded that the majority of substorm onsets do not take place in the vicinity of the Harang reversal. In fact, if substorm initiation proceeds simultaneously at two locations widely separated in MLT, it is highly unlikely that both locations are along the Harang reversal even though the Harang reversal may move or extend in MLT from premidnight, for example, depending on IMF B_Y (Rodger et al., 1984). This is most clear in the September 15, 2000 event (Section 2.1), in which the postmidnight auroral bulge formed in the dawn convection cell. The dawnside bulge was located in the dawn convection cell also in the March 18, 2001 event (Section 2.3 but convection map not shown). Therefore, although the Harang reversal may reflect the interchange stability of the corresponding magnetospheric structure, which is possibly subject to the substorm onset process (Ohtani et al., 2016), the onset location is probably not limited to the Harang reversal, and therefore, the convection reversal is not a requirement for the initiation of auroral substorms.

Second, our results also provide an important insight into the mapping of the WTS, an intense auroral enhancement forming at the duskside poleward edge of the auroral bulge. Whereas it is generally accepted that the WTS is an auroral manifestation of the upward FAC of the SCW (e.g., Fujii et al., 1994), its

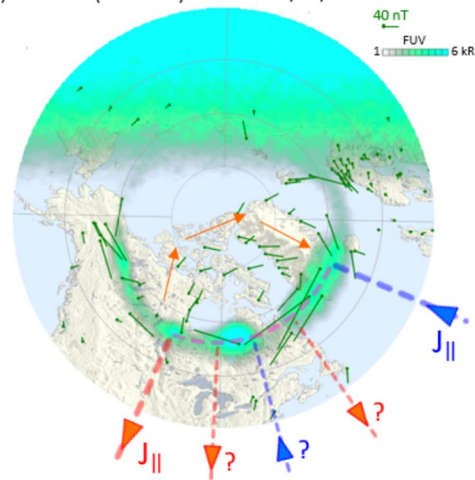
(a) 21:04:00 (21:03:44) UT on 2000/09/15



(b) 05:43:00 (05:42:28) UT on 2000/09/30



(c) 05:27:00 (05:26:26) UT on 2000/03/18



generation mechanism and mapping remain poorly understood. One previously proposed idea is that the WTS can be attributed to the shear flow instability at the duskside interface between the plasma sheet (PS) and low-latitude boundary layer (LLBL) (e.g., Rostoker, 1996). However, if two auroral bulges form simultaneously, it is very unlikely that both bulges map to this interface. This is especially so if one of the bulges is located in the dawn convection cell; note that for the dawnside PS-LLBL interface, the polarity of the associated FAC should be downward, rather than upward. The shear flow instability may be responsible for the formation of the WTS, and it may take place, if not always, at the duskside PS-LLBL interface, but the present study strongly suggests that this is not unique for the generation or mapping of the WTS.

Finally, we discuss the global M-I current system associated with the double auroral bulge formation. Figure 12 shows the polar map of equivalent currents at a selected time for each of the three events that we examined in Section 2. We note that in the September 30, 2000 (Figure 12b) and March 18, 2000 (Figure 12c) events, the equivalent currents swirled clockwise in the polar cap as guided by the red arrows. In general, a wedge current system results in a two-dimensional dipole-like configuration of equivalent currents (Fukushima, 1971), and this observed swirl can be considered as the poleward part of such a configuration. It is expected that a downward FAC feeds an enhanced westward auroral electrojet at postmidnight where the swirling equivalent current intersects with the auroral oval (thick blue dashed line), and an upward FAC drains this westward electrojet around its premidnight intersection (thick red dashed line). A similar structure can be found for the synoptic map of equivalent currents for isolated substorms (Gjerloev & Hoffman, 2014), and midlatitude positive bays are generally considered as its equatorward counterpart. That is, as a first approximation, the global M-I current system for those two events is represented by a single current wedge even though multiple auroral bulges formed.

This result, however, does not necessarily mean that a SCW did not form for individual auroral bulges in those events. Hypothetically speaking, if two wedge currents form side-by-side with the same intensity, their magnetic effects on the ground would be the same as those of a single current wedge that has the downward FAC of the dawnside current wedge and the upward FAC of the duskside current wedge. Gjerloev and Hoffman (2014) made a similar discussion for the possible disconnection of the SCW system around midnight for classical (i.e., Akasofu-type) isolated substorms. For our second (Figure 12b) and third (Figure 12c) events, the dawnside SCW can be associated with its own auroral bulge, and therefore, it is more likely that two distinct SCW systems coexisted in those events.

The pattern of equivalent currents is more complex for the September 15, 2000 event, which is shown in Figure 12a. Starting at the western end of the premidnight auroral enhancement, we can trace equivalent currents, which are directed northwest in the auroral zone and then proceed poleward along the terminator (see the red arrows). We can trace another stream line of equivalent currents, directed poleward along the midnight meridian. We suggest that these stream lines are parts of two coexisting swirls of equivalent currents and may share their dawnside half, which, however, is missing in Figure 12a because of sparse ground stations in the expected area. In other words, the nightside current system of this event appears to be represented by two current wedges that share the downward FAC but have their own upward FAC around the western end of each auroral bulge. However, this configuration of equivalent currents may also be understood in terms of two coexisting SCWs corresponding to individual auroral bulges (as we discussed for the second and third events) assuming that the dawnside SCW dominated the duskside one.

The above discussion of the global M-I current system versus two wedge currents is similar to the issue of whether the SCW is an ensemble of wedgelets, meso-scale wedge-like currents. In the present study, however, we selected events in which two auroral bulges developed simultaneously extending over a certain portion of the nightside auroral oval. Therefore, it is more likely that the corresponding M-I system is represented by a globally coherent current system. In contrast, for an individual auroral bulge, there is no necessity for wedgelets to form side-by-side with similar intensities and develop in parallel. Therefore, if the

Figure 12. Polar maps of equivalent currents (ground magnetic disturbance vectors rotated clockwise by 90°) at: (a) 2104 UT on September 15, 2000, (b) 0543 UT on September 30, 2000, and (c) 0527 UT on March 18, 2001 along with IMAGE FUV/WIC auroral images taken at the times in the parentheses. They are the same as Figures 2d, 6e, and 10f except that each map includes the day side, and the reference scale of the equivalent currents is 40 nT, instead of 100 nT. The red arrows guide the approximate direction of the equivalent currents. The dashed lines with arrows schematically show upward (red) and downward (blue) FACs expected from the distributions of equivalent currents and auroral bulges. The question marks indicate FACs expected from the auroral bulges but difficult to confirm with the equivalent currents. Those FACs are drawn as line currents for simplicity, but in reality they are volume currents.

SCW is an ensemble of wedgelets, the associated equivalent currents would not be globally coherent, which, however, is apparently the case for most isolated substorms (Ohtani & Gjerloev, 2020).

Back to Figure 12, we also note that in each event, the westward and eastward electrojets enhanced at dawn and dusk, respectively, indicating that another current system, which presumably corresponds to the global two-cell convection, coexisted along with the SCWs (Kamide & Kokubun, 1996). In the second event (Figure 12b), equivalent currents in the dawnside polar cap (see stations in Greenland) appear to deflect toward earlier MLTs than expected from a simple swirl. In the third event (Figure 12c), the polar-cap swirl of equivalent currents appear to extend further duskward of the postmidnight bulge reaching the duskside auroral intensification, which we interpret in terms of a convection enhancement rather than a substorm (Section 2.3). These features suggest that the substorm-related current system interplays with the current system associated with global convection. This remark is probably not exclusive to double-bulge events, but it should apply to auroral substorms in general (Ohtani et al., 2021).

4. Summary

In the present study we examined three substorm events in which the initial auroral intensification took place at more than one location leading to the simultaneous development of double auroral bulges. In those events each auroral bulge was accompanied by the enhancement of the westward auroral electrojet, and geosynchronous magnetic field dipolarized in the same sector as observed for ordinary substorms. Apparently two substorms took place simultaneously, although the two bulges later merged into one large bulge. The present result strongly suggests that substorm initiation is essentially a local process, and there is no global reference frame for substorm development. We also found that even if the SCW system formed for each of the two bulges, the polar map of equivalent currents can be represented by a global wedge system, and its structure is probably determined by the relative intensities and locations of the two SCWs.

Data Availability Statement

Ground magnetometer data from the Valentia, Brorfelde, and Borok stations were provided through the SuperMAG website (<http://supermag.jhuapl.edu/>) after its standard processing. Polar maps of equivalent currents along with IMAGA FUV/WIC data as well as the SMU and SML indices were also provided through the SuperMAG website. Polar maps of ionospheric convection were provided through the SuperDARN website at Virginia Tech (<http://vt.superdarn.org/tiki-index.php>). The GOES magnetometer data were provided by the National Centers for Environmental Information of National Oceanic and Atmospheric Administration (<http://www.ngdc.noaa.gov/stp/satellite/goes/dataaccess.html>). The OMNI data were provided by the GSFC/SPDF OMNIWeb at <https://omniweb.gsfc.nasa.gov>.

Acknowledgments

We thank the Irish Meteorological Service for the Valentia magnetometer data, Danish Technical University Space for the Brorfelde magnetometer data, Lancaster University for the Borok magnetometer data, the Geological Survey of Canada for the Poste de-la-Baleine magnetometer data, the CARISMA network for the Pinawa magnetometer data, and the United States Geological Survey for the Boulder magnetometer data. We also gratefully acknowledge that the SuperMAG indices and polar maps of equivalent currents used in this study were derived from data provided by many organizations and institutes as listed at <https://supermag.jhuapl.edu/info/?page=acknowledgement>. We are also grateful to the OMNI initiative for the OMNI data and NOAA for the GOES magnetometer data. Support for this research at the Johns Hopkins University Applied Physics Laboratory was provided by National Aeronautics and Space Administration (NASA) grants NNX16AF74G (SO) and NNX16AG74G (SO), National Science Foundation (NSF) grants 1502700 (SO), 1603028 (SO), and 1417899 (JWG).

References

- Ahn, B.-H., Kamide, Y., Kroehl, H. W., & Gorney, D. J. (1992). Cross-polar cap potential difference, auroral electrojet indices, and solar wind parameters. *Journal of Geophysical Research*, 97(A2), 1345–1352. <https://doi.org/10.1029/91JA02432>
- Akasofu, S.-I. (1964). The development of the auroral substorm. *Planetary and Space Science*, 12, 273. [https://doi.org/10.1016/0032-0633\(64\)90151-5](https://doi.org/10.1016/0032-0633(64)90151-5)
- Bristow, W. A., Greenwald, R. A., Shepherd, S. G., & Hughes, J. M. (2004). On the observed variability of the cross-polar cap potential. *Journal of Geophysical Research: Space Physics*, 109(A2). <https://doi.org/10.1029/2003JA012026>
- Bristow, W. A., & Jensen, P. (2007). A superposed epoch study of SuperDARN convection observations during substorms. *Journal of Geophysical Research: Space Physics*, 112(A6). <https://doi.org/10.1029/2006JA012049>
- Clauer, C. R., & McPherron, R. L. (1974). Mapping the local time-universal time development of magnetospheric substorms using mid-latitude magnetic observations. *Journal of Geophysical Research*, 79(19), 2811–2820. <https://doi.org/10.1029/JA079i019p02811>
- Frey, H. U., Mende, S. B., Angelopoulos, V., & Donovan, E. F. (2004). Substorm onset observations by IMAGE-FUV. *Journal of Geophysical Research: Space Physics*, 109(A10). <https://doi.org/10.1029/2004JA010607>
- Fujii, R., Hoffman, R. A., Anderson, P. C., Craven, J. D., Sugiura, M., Frank, L. A., & Maynard, N. C. (1994). Electrodynamics parameters in the nighttime sector during auroral substorms. *Journal of Geophysical Research: Space Physics*, 99(A4), 6093–6112. <https://doi.org/10.1029/93JA02210>
- Fukushima, N. (1971). Electric current systems for polar substorms and their magnetic effect below and above the ionosphere. *Radio Science*, 6, 269–275. <https://doi.org/10.1029/rs006i002p00269>
- Gjerloev, J. W. (2012). The SuperMAG data processing technique. *Journal of Geophysical Research: Space Physics*, 117(A9). <https://doi.org/10.1029/2012JA017683>

- Gjerloev, J. W., & Hoffman, R. A. (2001). The convection electric field in auroral substorms. *Journal of Geophysical Research: Space Physics*, 106(A7), 12919–12931. <https://doi.org/10.1029/1999JA000240>
- Gjerloev, J. W., & Hoffman, R. A. (2014). The large-scale current system during auroral substorms. *Journal of Geophysical Research: Space Physics*, 119(6), 4591–4606. <https://doi.org/10.1002/2013JA019176>
- Gjerloev, J. W., Hoffman, R. A., Sigwarth, J. B., & Frank, L. A. (2007). Statistical description of the bulge-type auroral substorm in the far ultraviolet. *Journal of Geophysical Research: Space Physics*, 112(A7). <https://doi.org/10.1029/2006JA012189>
- Greenwald, R. A., Baker, K. B., Hutchins, R. A., & Hanuise, C. (1985). An HF phased-array radar for studying small-scale structure in the high-latitude ionosphere. *Radio Science*, 20(1), 63–79. <https://doi.org/10.1029/rs020i001p00063>
- Kamide, Y., & Kokubun, S. (1996). Two-component auroral electrojet: Importance for substorm studies. *Journal of Geophysical Research: Space Physics*, 101(A6), 13027–13046. <https://doi.org/10.1029/96JA00142>
- Kepko, L., McPherron, R. L., Amm, O., Apatenkov, S., Baumjohann, W., Birn, J., et al. (2015). Substorm current wedge revisited. *Space Science Reviews*, 190, 1–46. <https://doi.org/10.1007/s11214-014-0124-9>
- Liou, K., Newell, P. T., Sibeck, D. G., Meng, C.-I., Brittnacher, M., & Parks, G. (2001). Observation of IMF and seasonal effects in the location of auroral substorm onset. *Journal of Geophysical Research: Space Physics*, 106(A4), 5799–5810. <https://doi.org/10.1029/2000JA003001>
- Lopez, R. E., & von Rosenvinge, T. (1993). A statistical relationship between the geosynchronous magnetic field and substorm electrojet magnitude. *Journal of Geophysical Research: Space Physics*, 98(A3), 3851–3857. <https://doi.org/10.1029/92JA01660>
- Mende, S. B., Heetderks, H., Frey, H. U., Stock, J. M., Lampton, M., Geller, S. P., et al. (2000). Far ultraviolet imaging from the Image Spacecraft. 3. Spectral Imaging of Lyman- α and OI 135.6 nm. *Space Science Reviews*, 91, 287. https://doi.org/10.1007/978-94-011-4233-5_10
- Nagata, T., & Fukushima, N. (1971). Morphology of magnetic disturbance. In *Encyclopedia of physics (Handbuch der Physik)*, *Geophysics III (Part III)* (Vol. 49/3, pp. 5–130). Springer.
- Newell, P. T., & Gjerloev, J. W. (2011). Evaluation of SuperMAG auroral electrojet indices as indicators of substorms and auroral power. *Journal of Geophysical Research: Space Physics*, 116(A12). <https://doi.org/10.1029/2011JA016779>
- Ohtani, S. (2019). Substorm energy transport from the magnetotail to the nightside ionosphere. *Journal of Geophysical Research: Space Physics*, 124. <https://doi.org/10.1029/2019ja026964>
- Ohtani, S., & Gjerloev, J. W. (2020). Is the substorm current wedge an ensemble of wedgelets?: Revisit to midlatitude positive bays. *Journal of Geophysical Research: Space Physics*, 125. <https://doi.org/10.1029/2020ja027902>
- Ohtani, S., Gkioulidou, M., Wang, C. P., & Wolf, R. A. (2016). The Harang reversal and the interchange stability of the magnetotail. *Journal of Geophysical Research: Space Physics*, 121, 3278–3292. <https://doi.org/10.1002/2015JA022025>
- Ohtani, S., Imajo, S., Nakamizo, A., & Gjerloev, J. W. (2021). Globally correlated ground magnetic disturbances, during substorms. *Journal of Geophysical Research: Space Physics*, 126. <https://doi.org/10.1029/2020ja028599>
- Rodger, A. S., Cowley, S. W. H., Brown, M. J., Pinnock, M., & Simmons, D. A. (1984). Dawn-dusk (y) component of the interplanetary magnetic field and the local time of the Harang discontinuity. *Planetary and Space Science*, 32(8), 1021–1027. [https://doi.org/10.1016/0032-0633\(84\)90058-8](https://doi.org/10.1016/0032-0633(84)90058-8)
- Rostoker, G. (1996). Phenomenology and physics of magnetospheric substorms. *Journal of Geophysical Research: Space Physics*, 101(A6), 12955–12973. <https://doi.org/10.1029/96JA00127>
- Ruohoniemi, J. M., & Baker, K. B. (1998). Large-scale imaging of high-latitude convection with Super Dual Auroral Radar Network HF radar observations. *Journal of Geophysical Research: Space Physics*, 103(A9), 2079720811. <https://doi.org/10.1029/98ja01288>
- Shue, J.-H., Newell, P. T., Liou, K., Meng, C.-I., Kamide, Y., & Lepping, R. P. (2002). Two-component auroras. *Geophysical Research Letters*, 29(10), 17. <https://doi.org/10.1029/2002GL014657>
- Tsyganenko, N. A. (1989). A magnetospheric magnetic field model with a warped tail current sheet. *Planetary and Space Science*, 37, 5. [https://doi.org/10.1016/0032-0633\(89\)90066-4](https://doi.org/10.1016/0032-0633(89)90066-4)
- Weygand, J. M., McPherron, R. L., Frey, H. U., Amm, O., Kauristie, K., Viljanen, A., & Koistinen, A. (2008). Relation of substorm onset to Harang discontinuity. *Journal of Geophysical Research: Space Physics*, 113(A4). <https://doi.org/10.1029/2007JA012537>
- Wolf, R. A., Wan, Y., Xing, X., Zhang, J.-C., & Sazykin, S. (2009). Entropy and plasma sheet transport. *Journal of Geophysical Research: Space Physics*, 114(A9). <https://doi.org/10.1029/2009JA014044>
- Zou, S., Lyons, L. R., Wang, C.-P., Boudouridis, A., Ruohoniemi, J. M., Anderson, P. C., et al. (2009). On the coupling between the Harang reversal evolution and substorm dynamics: A synthesis of SuperDARN, DMSP, and IMAGE observations. *Journal of Geophysical Research: Space Physics*, 114(A1). <https://doi.org/10.1029/2008JA013449>